The Weighted Markov-Dubins Problem

Deepak Prakash Kumar, Swaroop Darbha, *Fellow, IEEE*, Satyanarayana Gupta Manyam, *Member, IEEE*, and David Casbeer, *Senior Member, IEEE*

***Abstract*—In this letter, a variation of the classical Markov-Dubins problem is considered, which deals with curvature-constrained least-cost paths in a plane with prescribed initial and final configurations, different bounds for the sinistral and dextral curvatures, and penalties μ_L and μ_R for the sinistral and dextral turns, respectively. The addressed problem generalizes the classical Markov-Dubins problem and the asymmetric sinistral/dextral Markov-Dubins problem. The proposed formulation can be used to model an Unmanned Aerial Vehicle (UAV) with a penalty associated with a turn due to the required additional thrust to maintain altitude and airspeed while turning, or a UAV with different curvature bounds and costs for the sinistral and dextral turns due to hardware failures. Using optimal control theory, the main result of this letter shows that the optimal path belongs to a set of at most 21 candidate paths, each comprising of at most five segments. Unlike in the classical Markov-Dubins problem, the CCC path, which is a candidate path for the classical Markov-Dubins problem, is not optimal for the weighted Markov-Dubins problem. Moreover, the obtained list of candidate paths for the weighted Markov-Dubins problem reduces to the standard CSC and CCC paths and the corresponding degenerate paths when μ_L and μ_R approach zero.**

***Index Terms*—Aerial systems: Applications, optimization and optimal control, motion and path planning.**

I. Introduction

AUTONOMOUS vehicles, which includes UAVs, have increasing military and civilian applications, thereby increasing the need for path planning for various scenarios that the vehicles might encounter. Path planning for UAVs is typically addressed by modeling the vehicle as a Dubins vehicle, wherein the vehicle travels forward at a constant speed and has a constraint on the curvature of the path. The classical Markov-Dubins problem, which addresses the curvature-constrained planar paths of shortest length connecting given initial and final configurations, was solved in [1]. For this problem, the optimal paths were obtained as CSC and CCC paths and degenerate paths of the same. Here, $C \in \{L, R\}$ represents a sinistral (L) or a dextral (R) turn, respectively, of minimum turning radius, and S represents a straight line segment. A variation of the Markov-Dubins problem was studied in [2], wherein the vehicle was allowed to move forwards or backward. Such a vehicle is referred to as a Reeds-Shepp vehicle.

Results in [1] and [2] were proved without resorting to Pontryagin's Minimum Principle (PMP). The Markov-Dubins problem and path planning for the Reeds-Shepp vehicle were approached using PMP [3] to characterize the optimal path systematically in [4] and [5], respectively. Recently, in [6], the Markov-Dubins problem was approached using both PMP and phase portraits to simplify the proofs further. Using the obtained candidate optimal paths through one of the discussed approaches, the path synthesis problem is then addressed to determine the optimal path given initial and final configurations. Path synthesis for the Markov-Dubins problem has been addressed in [7], [8], while [9] addresses the same problem for the Reeds-Shepp vehicle.

In the literature, various extensions/variations of the Markov-Dubins problem have been studied. For example, [10] and [11] investigate the Markov-Dubins problem on a Riemann manifold and 3D, respectively. In [12], the shortest curvature-constrained paths for a UAV to pursue a target moving on a circle is considered. The asymmetric sinistral/dextral Markov-Dubins problem is addressed in [13], wherein the bound on the sinistral and dextral curvatures need not be the same. This study obtained the same set of candidate paths as the classical Markov-Dubins problem, with the difference arising in the path synthesis. The motivation of the study was to plan optimal paths for a UAV with a turn preference due to hardware failures such as damage to an aileron, which is responsible for turning the vehicle [14]. However, considering different bounds for the sinistral and dextral curvatures cannot completely capture the turn preference of the UAV. Hence, a weighted Markov-Dubins problem is addressed in this study, wherein different bounds for the sinistral and dextral curvatures, and penalties μ_L and μ_R are considered for sinistral and dextral turns, respectively. Furthermore, for UAVs with the same bound on the sinistral and dextral curvatures, the weighted Markov-Dubins framework penalizes the turns to account for the additional thrust required to maintain the same altitude and airspeed during a turn [15].

Application of Pontryagin's minimum principle to the weighted Markov-Dubins problem yields a total of 21 candidate optimal paths, wherein each path has at most five segments. Moreover, when $\mu_L = \mu_R = 0$, the candidate paths reduce to CSC and CCC paths and corresponding degenerate paths. Therefore, the proposed weighted Markov-Dubins problem generalizes the classical Markov-Dubins problem [1], [5] and the asymmetric sinistral/dextral Markov-Dubins problem [13].

Manuscript received 24 August 2022; accepted 1 January 2023. Date of publication 23 January 2023; date of current version 7 February 2023. This letter was recommended for publication by Associate Editor K. Leahy and Editor A. Bera upon evaluation of the reviewers' comments. *(Corresponding author: Satyanarayana Gupta Manyam.)*

Deepak Prakash Kumar and Swaroop Darbha are with the Department of Mechanical Engineering, Texas A&M University, College Station, TX 77843 USA (e-mail: deepakprakash1997@gmail.com; dswaroop@tamu.edu).

Satyanarayana Gupta Manyam is with Infoscitex Corp., Dayton, OH 45431 USA (e-mail: msngupta@gmail.com).

David Casbeer is with Autonomous Control Branch, Air Force Research Laboratory, Wright-Patterson Air Force Base, OH 45433 USA (e-mail: david.casbeer@us.af.mil).

Digital Object Identifier 10.1109/LRA.2023.3239316

The contributions of this letter are:

i) Formulation of the proposed weighted Markov-Dubins problem as an optimal control problem and solving it using Pontryagin's minimum principle,
ii) Proving non-optimality of six-segment paths, thereby proving optimal paths can contain at most five segments, and
iii) Simulations to study the effect of different parameters and configurations on the type of optimal path obtained and the differences from the classical and asymmetric sinistral/dextral Markov-Dubins problems.

The rest of the article is organized as follows. In Section II, the problem formulation for the weighted Markov-Dubins problem is presented. In Section III, the candidate paths for the least-cost path connecting given initial and final configurations are identified using PMP and phase portraits. In Section IV, a typical case for the classical Markov-Dubins problem is analyzed without and with penalties, and simulation results on the effect of parameters and configurations on the optimal path are discussed. Finally, conclusions are presented in Section V.

II. Problem Formulation

In this letter, the least-cost path problem for a curvature-constrained planar vehicle with different sinistral and dextral curvatures with given initial and final configurations is considered. In contrast to [13], penalties μ_L and μ_R are allocated to sinistral and dextral turns, respectively. Consider a bounded control input $u(t) \in [-U_R, U_L]$, which controls the rate of change of the vehicle's heading angle. Therefore, the kinematic equations for the vehicle are given by

$$\dot{x}(t) = \cos\alpha(t),\ \dot{y}(t) = \sin\alpha(t),\ \dot{\alpha}(t) = u(t), \tag{1}$$

where x, y are the Cartesian coordinates for the vehicle, and α denotes the heading angle of the vehicle. It should be noted here that if $u > 0$, the vehicle takes a sinistral (left) turn, and if $u < 0$, the vehicle takes a dextral (right) turn.

Equation (1) can alternatively be written in terms of two control inputs $u_L(t) \in [0, U_L]$ and $u_R(t) \in [0, U_R]$, which denote the rate of change of the vehicle's heading angle corresponding to left and right turns, respectively. Consider weights μ_L, μ_R that penalize the left and right turns, respectively, such that $\mu_L, \mu_R \geq 0$ and at least one of the penalties is non-zero, i.e., $\mu_L + \mu_R > 0$. The minimum cost path problem can be formulated as

$$\min \int_0^{t_f} (1 + \mu_L u_L(t) + \mu_R u_R(t))dt, \tag{2}$$

subject to

$$\dot{x}(t) = \cos\alpha(t),\ \dot{y}(t) = \sin\alpha(t),\ \dot{\alpha}(t) = u_L(t) - u_R(t), \tag{3}$$

$$(u_L(t), u_R(t)) \in [0, U_L] \times [0, U_R], \tag{4}$$

$$x(0) = x_i,\ y(0) = y_i,\ \alpha(0) = \alpha_i, \tag{5}$$

$$x(t_f) = x_f,\ y(t_f) = y_f,\ \alpha(t_f) = \alpha_f. \tag{6}$$

In the formulation, t_f is the final free time, (3) represents the modified kinematics equation in (1) with u_L and u_R as the control inputs, and (4) represents the range of the control inputs. Moreover, (5) and (6) denote the boundary conditions, which are the given initial and final configurations, respectively.

The above formulation represents a generalization of the time-fuel problem [16]. In the time-fuel problem, the cost to be minimized is $J_f = \int_0^{t_f} (\mu_0 + \mu|u|)dt$, where $|u| \leq U$ and $\mu_0 + \mu|u|$ represents fuel used during a turn. As μ_0 represents the fuel used over a straight line segment, $\mu_0 \neq 0$. Setting $U_L = U_R = U$ and $\mu_L = \mu_R = \frac{\mu}{\mu_0}$ in (2) yields an objective functional equivalent to $\frac{1}{\mu_0} J_f$.

III. Characterization of the Optimal Paths

In this section, the optimal path for the presented problem formulation will be characterized using Pontryagin's minimum principle (PMP). Declaring e, p, q, and β to be the adjoint variables associated with the integrand in (2) and the three kinematic constraints in (3), respectively, the Hamiltonian H is given by

$$\begin{aligned} H = {} & e(1 + \mu_L u_L(t) + \mu_R u_R(t)) + p(t)\cos\alpha(t) \\ & + q(t)\sin\alpha(t) + \beta(t)\left(u_L(t) - u_R(t)\right), \end{aligned} \tag{7}$$

where the dependence of H on the states x, y, and α, the adjoint variables, and the control inputs is not shown for brevity. The rate of change of adjoint variables is given by

$$\begin{aligned} \dot{p}(t) &= -\frac{\partial H}{\partial x(t)} = 0, \quad \dot{q}(t) = -\frac{\partial H}{\partial y(t)} = 0, \\ \dot{\beta}(t) &= -\frac{\partial H}{\partial \alpha(t)} = p(t)\sin\alpha(t) - q(t)\cos\alpha(t). \end{aligned} \tag{8}$$

Defining $\lambda = \sqrt{p^2 + q^2}$ and $\tan\phi = \frac{q}{p}$, the Hamiltonian and the equations for the adjoint variables can be written as

$$\begin{aligned} H = {} & e + (\beta(t) + \mu_L e)\, u_L(t) + (\mu_R e - \beta(t))\, u_R(t) \\ & + \lambda\cos(\alpha(t) - \phi), \end{aligned} \tag{9}$$

$$p = \lambda\cos\phi,\ q = \lambda\sin\phi,\ \dot{\beta}(t) = \lambda\sin(\alpha(t) - \phi). \tag{10}$$

It should be noted that from PMP, e is a constant and $e \geq 0$. Moreover, for the problem formulation presented, the optimal control actions correspond to $H \equiv 0$ [17].

Lemma 1: The optimal control actions are given by $(u_L, u_R) \in \mathcal{U} = \{(0,0), (U_L, 0), (0, U_R)\}$.

Proof: From the Hamiltonian given in (9), and for it to be minimum, the following conditions should hold:

$$(\beta(t) + \mu_L e)\, u_L(t) \leq 0,\ (\mu_R e - \beta(t))\, u_R(t) \leq 0. \tag{11}$$

Further, either of the two cases holds:

- $\frac{\partial H}{\partial u_L} = \beta(t) + \mu_L e \equiv 0$ or $\frac{\partial H}{\partial u_R} = \mu_R e - \beta(t) \equiv 0$. This implies that β is a constant, and therefore, $\dot{\beta}(t) \equiv 0$. Consequently, $\lambda\sin(\alpha(t) - \phi) \equiv 0$. If $\lambda = 0$, e should be equal to zero as in (9), $H \equiv 0$, $u_L, u_R \geq 0$, $\mu_L, \mu_R \geq 0$ with $\mu_L + \mu_R > 0$. Therefore, $\beta(t) \equiv 0$. Hence, $(e, p, q, \beta) \equiv \mathbf{0}$, which violates the nontriviality condition of PMP. Hence, $\dot{\beta}(t) \equiv 0 \Rightarrow \sin(\alpha(t) - \phi) \equiv 0$. Therefore, $\alpha(t) \equiv \phi$ or $\alpha(t) \equiv \phi + \pi$. Hence, the path is a straight line segment.

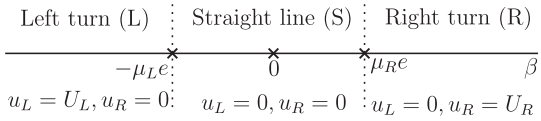

Fig. 1. Control action depending on the value of β.

- $\frac{\partial H}{\partial u_L} \not\equiv 0$ and $\frac{\partial H}{\partial u_R} \not\equiv 0$. Three types of control actions arise depending on the value of β using (11), which are depicted in Fig. 1.

For a more detailed proof, the reader may refer to [18]. ■

Proposition 2: Any optimal path is a concatenation of arcs of circles of radius r_L corresponding to a left turn and r_R corresponding to a right turn, and straight line segments.

Henceforth, a left turn segment will be denoted by L, a right turn segment will be denoted by R, and a straight line segment by S. Moreover, a segment corresponding to a turn will be denoted by C.

Using Fig. 1 and noting that β is continuous, the observations made are given in the following proposition and lemma.

Proposition 3: The value of β corresponding to the inflection point of a CS or SC subpath of an optimal path is as follows:

1) At the inflection point of an LS or SL subpath, $\beta = -\mu_L e$.
2) At the inflection point of an RS or SR subpath, $\beta = \mu_R e$.

Lemma 4: An optimal path can contain an LR or RL subpath if $e = 0$ and at the inflection point, $\beta = 0$.

Proof: The proof follows from the value of β for L and R segments, which are shown in Fig. 1, and continuity of β. For a more detailed proof, the reader may refer to [18]. ■

The candidate paths for an optimal path will be obtained using a phase portrait approach. Among the adjoint variables, β is the only time-varying adjoint variable. Moreover, the control actions, and therefore, the segments of an optimal path, depend on the trajectory of β. Hence, the phase portrait of β can be used to determine the candidate paths. To this end, an equation relating β and $\dot{\beta}$ is first obtained. To obtain this relation, the Heaviside function, θ, defined below, is used:

$$\theta(\eta) = \begin{cases} 1, & \eta \geq 0, \\ 0, & \eta < 0. \end{cases}$$

From (9), noting that $H \equiv 0$, $\lambda \cos(\alpha(t) - \phi)$ can be obtained. Using the obtained expression, noting that $u_L = U_L \theta(-\beta(t) - \mu_L e)$, $u_R = U_R \theta(\beta(t) - \mu_R e)$, and using the expression for $\dot{\beta}$ from (10), β and $\dot{\beta}$ are related by

$$\Big(e + (\beta(t) + \mu_L e)\, U_L \theta\left(-\beta(t) - \mu_L e\right) + (\mu_R e - \beta(t))\, U_R \theta\left(\beta(t) - \mu_R e\right)\Big)^2 + \dot{\beta}^2(t) = \lambda^2. \quad (12)$$

In the above equation, the parameters r_L, r_R, μ_L, and μ_R correspond to the vehicle; the relation between β and $\dot{\beta}$ depends on e and λ. As e and λ are constants for a given path, the complete list of candidate paths can be obtained from the following cases:

- Case 1: $e = 0$. The solutions obtained are abnormal solutions as they are independent of the objective functional given in (2).

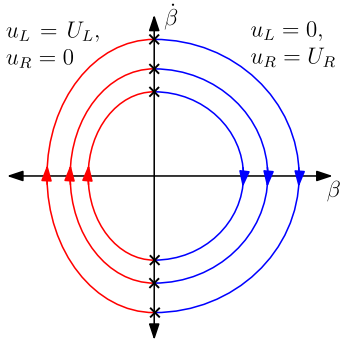

Fig. 2. Phase portrait of β for $e = 0$.

- Case 2: $e > 0$. In this case, e can be set to one without loss of generality, as it leads to a corresponding scaling of λ, β, and consequently, $\dot{\beta}$. Three sub-cases arise depending on the value of λ:
  - Case 2.1: $\lambda < e = 1$.
  - Case 2.2: $\lambda = e = 1$.
  - Case 2.3: $\lambda > e = 1$.

The obtained solutions for each of these cases are derived in the following subsections.

A. Candidate Paths for $e = 0$

When $e = 0$, (12) reduces to

$$\left(\beta(t) U_L \theta\left(-\beta(t)\right) - \beta(t) U_R \theta\left(\beta(t)\right)\right)^2 + \dot{\beta}^2(t) = \lambda^2. \quad (13)$$

Lemma 5: If $e = 0$, then $\lambda > 0$.

Proof: If $e = 0$ and $\lambda = 0$, the only solution for β satisfying (13) is $\beta(t) \equiv 0$. However, the nontriviality condition of PMP is violated as all adjoint variables are identically equal to zero. Therefore, $e = 0 \Rightarrow \lambda > 0$. For a more detailed proof, the reader may refer to [18]. ■

Equation (13) can be expressed explicitly as:

$$f\left(\beta(t), \dot{\beta}(t)\right) = \begin{cases} \left(\frac{\beta(t)}{r_L}\right)^2 + \dot{\beta}^2(t) = \lambda^2, & \beta(t) < 0 \\ \dot{\beta}^2(t) = \lambda^2, & \beta(t) = 0, \\ \left(\frac{\beta(t)}{r_R}\right)^2 + \dot{\beta}^2(t) = \lambda^2, & \beta(t) > 0 \end{cases} \quad (14)$$

since $U_L = \frac{1}{r_L}$ and $U_R = \frac{1}{r_R}$. The phase portrait obtained for β using the above defined function is shown in Fig. 2. Since $e = 0$, from the proof of Lemma 1 and Fig. 1, an S segment exists over a time interval $\mathcal{I}$ of the path only when $\beta(t) = 0$ for $t \in \mathcal{I}$. Since $\dot{\beta}(t) = \pm\lambda$ when $\beta(t) = 0$ from (14), an S segment is not a part of an optimal path for $e = 0$. Hence, $(\beta(t), \dot{\beta}(t)) \in \{(0, \lambda), (0, -\lambda)\}$ is an inflection point between two C segments. Therefore, for $e = 0$, candidate optimal paths are concatenations of C segments.

Remark 1: A non-trivial path is defined as a path wherein all subpaths have a non-zero length.

Theorem 6: For $e = 0$, a non-trivial CCC path is non-optimal.

Proof: It suffices to consider the non-optimality of an LRL path. If it were optimal, let the time instants corresponding to

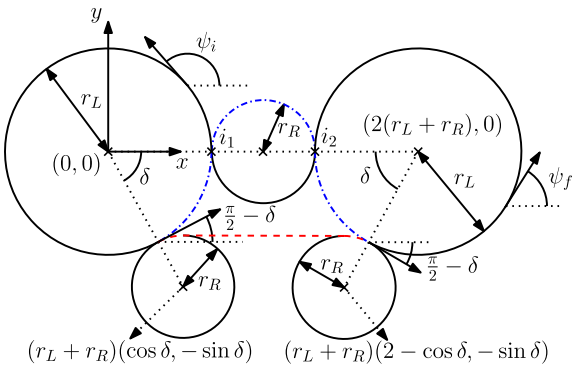

Fig. 3. Non-optimality of an $L_\alpha R_\pi L_\gamma$ path.

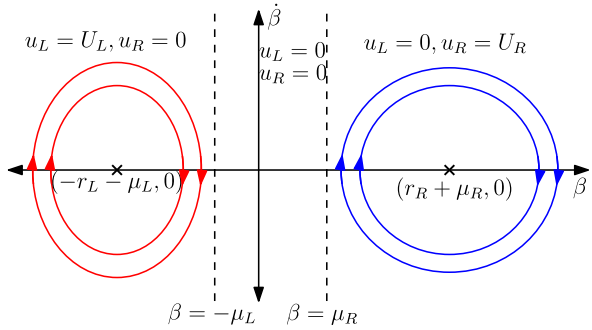

Fig. 4. Phase portrait of β for $\lambda < e = 1$.

the first and second inflection points be t_1 and t_2, respectively. From Figs. 1 and 2, $(\beta(t_1), \dot\beta(t_1)) = (0, \lambda)$ and $(\beta(t_2), \dot\beta(t_2)) = (0, -\lambda)$. As $\dot\beta(t) = \lambda \sin(\alpha(t) - \phi)$, $\lambda > 0$ from Lemma 5, and $\dot\beta(t_1) = -\dot\beta(t_2) = \lambda$, $\alpha(t_1)$ and $\alpha(t_2)$ are separated by an odd multiple of π. As a similar argument applies for an RLR path, it is sufficient to consider a non-trivial $CC_\pi C$ path.

Consider an $L_\alpha R_\pi L_\gamma$ path, where $\alpha, \gamma > 0$. Without loss of generality, let the circle corresponding to the L_α segment be located at the origin, as shown in Fig. 3. As the middle arc angle is π, the center of the circle of the L_γ segment can be placed along the x-axis without loss of generality. Consider an $L_\delta R_\pi L_\delta$ subpath, where $0 < \delta < \min(\alpha, \gamma, \frac{\pi}{2})$. It is claimed that an alternate RSR path, shown in Fig. 3 using dashed lines, can be constructed at a lower cost than the $L_\delta R_\pi L_\delta$ subpath (shown using dash-dotted lines).

From Fig. 3, the length of the line segment (l_S) of the RSR path can be obtained as $2(r_L + r_R)(1 - \cos\delta)$. Moreover, from this figure, it can be observed that the angle of turn for each R segment equals $\frac{\pi}{2} - \delta$, as the S segment is parallel to the $x-$axis. The cost difference between the $L_\delta R_\pi L_\delta$ subpath and the $R_{\frac{\pi}{2}-\delta} S_{l_S} R_{\frac{\pi}{2}-\delta}$ path is given by

$$\begin{aligned}\Delta c &= c_{L_\delta R_\pi L_\delta} - c_{R_{\frac{\pi}{2}-\delta} S_{l_S} R_{\frac{\pi}{2}-\delta}} \\ &= 2(c_L + c_R)\delta - 2c_S(r_L + r_R)(1 - \cos\delta), \end{aligned} \tag{15}$$

where c_L, c_R, and c_S are costs associated with the L, R, and S segments, respectively. The derivation of these costs follows.

Using (2), the total cost C_L of a left turn can be obtained as a function of the angle of the turn (ϕ_L) by setting $u_L = U_L = \frac{1}{r_L}$ and $u_R = 0$ as $C_L = (r_L + \mu_L)\phi_L$, as the vehicle is considered to move at a unit speed. Therefore, $c_L = r_L + \mu_L$. Similarly, c_R and c_S can be obtained as $r_R + \mu_R$ and 1, respectively. Substituting the obtained expressions for c_L, c_R, and c_S in (15), a lower bound for Δc can be obtained as

$$\Delta c > 2(r_L + r_R)(\delta + \cos\delta - 1), \tag{16}$$

as $\mu_L, \mu_R \geq 0$ with $\mu_L + \mu_R > 0$.

Consider the function $g(\delta) := \delta + \cos\delta - 1$. This function is positive $\forall \delta \in (0, \frac{\pi}{2})$ as

1) $g(0) = 0$, and
2) $\frac{dg}{d\delta} = 1 - \sin\delta > 0 \, \forall \, \delta \in [0, \frac{\pi}{2})$, which implies that g is strictly increasing in this range.

Therefore, $\Delta c > 0 \, \forall \, \delta \in (0, \frac{\pi}{2})$. Hence, the $R_{\frac{\pi}{2}-\delta} S_{l_S} R_{\frac{\pi}{2}-\delta}$ path can replace the $L_\delta R_\pi L_\delta$ subpath of the $L_\alpha R_\pi L_\gamma$ path at a lower cost. Therefore, the $L_\alpha R_\pi L_\gamma$ path is not optimal. A similar argument can be made for an $R_\alpha L_\pi R_\gamma$ path. Hence, for $e = 0$, a CCC path is non-optimal. For a more detailed proof, the reader may refer to [18]. ■

Proposition 7: For $e = 0$, the optimal path candidates are C and CC, wherein the angle of each segment is at most π.

B. Candidate Paths for $\lambda < e = 1$

When $e = 1$, equation (12) can be expressed as

$$f\left(\beta(t), \dot\beta(t)\right) = \begin{cases} \left(\frac{r_L+\mu_L}{r_L} + \frac{\beta(t)}{r_L}\right)^2 + \dot\beta^2(t) = \lambda^2, & \beta(t) < -\mu_L \\ \dot\beta^2(t) = \lambda^2 - 1, & -\mu_L \leq \beta(t) \leq \mu_R \\ \left(\frac{r_R+\mu_R}{r_R} - \frac{\beta(t)}{r_R}\right)^2 + \dot\beta^2(t) = \lambda^2, & \beta(t) > \mu_R \end{cases}. \tag{17}$$

If $\lambda < 1$, $\dot\beta(t)$ does not have a real solution for $-\mu_L \leq \beta \leq \mu_R$; hence, the initial condition for β cannot lie in $[-\mu_L, \mu_R]$. The following lemma will also establish that for any other initial condition, $\beta(t) \notin [-\mu_L, \mu_R]$ for any $t > 0$.

Lemma 8: For $\lambda < e = 1$, if $\beta(0) < -\mu_L$, then $\beta(t) < -\mu_L$, $\forall \, t > 0$. If $\beta(0) > \mu_R$, then $\beta(t) > \mu_R$, $\forall \, t > 0$.

Proof: Suppose $\beta(0) + \mu_L < 0$; should $\beta(t) + \mu_L = 0$ for any t, equation (17) implies that $1 \leq 1 + \dot\beta^2(t) = \lambda^2 < 1$, a contradiction; hence, $\beta(t) + \mu_L < 0$ for all t by continuity of β. A similar reasoning can be used to show that $\beta(0) - \mu_R > 0 \Rightarrow \beta(t) - \mu_R > 0$ for all $t > 0$. ■

The phase portrait obtained for $\lambda < e = 1$ using (17) and the previous observations is shown in Fig. 4. Using Lemma 8 and Fig. 4, it can be observed that the only candidate path is C for $\lambda < e = 1$.

C. Candidate Paths for $\lambda = e = 1$

The equation corresponding to $\beta(t) < -\mu_L$ in (17) corresponds to an ellipse, whose origin lies on the $\beta-$axis. The intersection points of this ellipse with the $\beta-$axis are at $\beta = (\pm\lambda - 1)r_L - \mu_L$. For $\lambda = 1$, the intersection points are at $\beta = -\mu_L$ and $\beta = -2r_L - \mu_L$. Hence, this ellipse is tangential

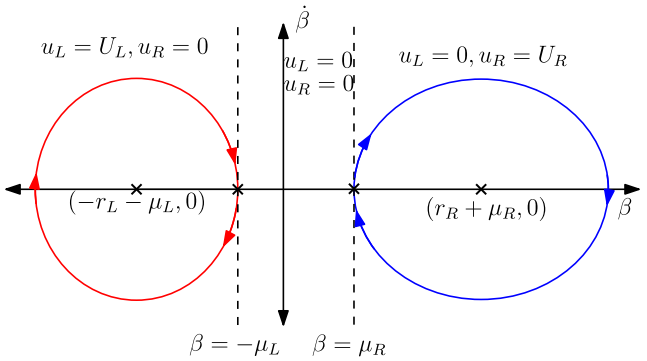

Fig. 5. Phase portrait of β for $\lambda = e = 1$.

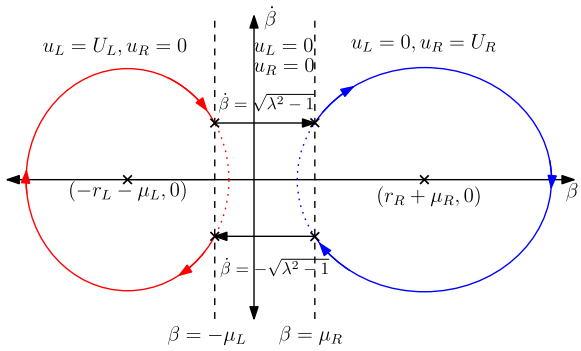

Fig. 6. Phase portrait of β for $\lambda > e = 1$.

to the line $\beta = -\mu_L$. Similarly, the ellipse corresponding to $\beta(t) > \mu_R$ can be observed to be tangential to the line $\beta = \mu_R$. It should also be noted that when $\lambda = 1$, $\dot{\beta}(t) = 0$ for $-\mu_L \leq \beta(t) \leq \mu_R$ from (17). Using these observations and (17), the phase portrait for β for $\lambda = e = 1$ can be obtained as shown in Fig. 5. The candidate paths for $\lambda = e = 1$ can be obtained using the following lemma.

Lemma 9: For $\lambda = e = 1$, the optimal path is LSL, RSR, or a degenerate path of LSL and RSR paths.

Proof: Let $\beta(0) \leq -\mu_L$. From (17) and Fig. 5, if $\beta(t) < -\mu_L$, the evolution of β corresponds to an ellipse, and if $\beta(t) = -\mu_L$, then $\dot{\beta}(t) = 0$. Hence, $\beta(0) \leq -\mu_L \Rightarrow \beta(t) \leq -\mu_L \, \forall \, t > 0$. As $\beta(t) = -\mu_L \Rightarrow \dot{\beta}(t) = 0$, $\beta(t)$ can be identically equal to $-\mu_L$ over a time interval, which corresponds to an S segment from Lemma 1. Hence, the optimal path has alternate L and S segments.

Consider an SLS path. Here, $\beta(0) = -\mu_L$, $\beta(t_f) = -\mu_L$. Since $\dot{\beta} = \lambda \sin(\alpha(t) - \phi)$, and at the inflection points, $\beta = -\mu_L$ and $\dot{\beta} = 0$, the angle of the L segment is a multiple of 2π. Hence, an SLS path is not optimal. Therefore, if $\beta(0) \leq -\mu_L$, the candidate paths are S, L, LS, SL, and LSL.

Using a similar argument for $\beta(0) \geq \mu_R$, the candidate paths can be obtained as S, R, RS, SR, and RSR. If $\beta(0) \in (-\mu_L, \mu_R)$, $\beta(t) = \beta(0) \, \forall \, t > 0$ as $\dot{\beta} = 0$ from (17). Using Lemma 1, the optimal path in this scenario is S. ■

D. Candidate Paths for $\lambda > e = 1$

As the intersection points of the ellipse corresponding to $\beta(t) < -\mu_L$ with the $\beta-$axis are at $\beta = (\pm\lambda - 1)r_L - \mu_L$, for $\lambda > 1$, one of the intersection points lies to the right of the line $\beta = -\mu_L$. Therefore, the ellipse corresponding to $\beta(t) < -\mu_L$ intersects with the line $\beta = -\mu_L$ at two points. The coordinates of these two points can be obtained from (17) as $(-\mu_L, \pm\sqrt{\lambda^2 - 1})$. Similarly, the ellipse corresponding to $\beta(t) > \mu_R$ can be observed to intersect the line $\beta = \mu_R$ at two points, whose coordinates are given by $(\mu_R, \pm\sqrt{\lambda^2 - 1})$. Moreover, for $-\mu_L \leq \beta(t) \leq \mu_R$, $\dot{\beta}(t) = \pm\sqrt{\lambda^2 - 1}$ from (17). Using these observations and (17), the phase portrait for β for $\lambda > e = 1$ can be obtained as shown in Fig. 6. From this figure, the following proposition follows.

Proposition 10: The segments of an optimal path for $\lambda > e = 1$ is a cyclic permutation of L, S_1, R, and S_2 segments, wherein

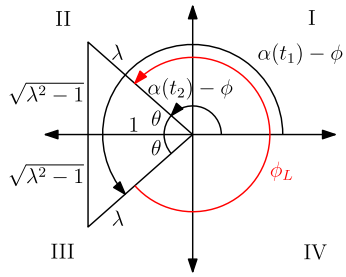

Fig. 7. Angle of an L segment for an optimal SLS path for $\lambda > e = 1$.

S_1 and S_2 denote straight line segments with $\dot{\beta}(t) = \sqrt{\lambda^2 - 1}$ and $\dot{\beta}(t) = -\sqrt{\lambda^2 - 1}$, respectively.

Corollary 11: For $\lambda > e = 1$, a non-trivial CC path is non-optimal.

It should be noted that henceforth, both S_1 and S_2 segments will be denoted as an S segment. Using the sequence of segments in an optimal path given in Proposition 10 and Fig. 6, it is easy to deduce whether an S segment denotes an S_1 or S_2 segment in an optimal path.

Lemma 12: For $\lambda > e = 1$, the angle of the C segment of a non-trivial optimal SCS path is $2\pi - 2\cos^{-1}(\frac{1}{\lambda})$.

Proof: Let a non-trivial SLS path be optimal, for which the first and second inflection points occur at time instants t_1 and t_2, respectively. Hence, $\beta(t_1) = \beta(t_2) = -\mu_L$, and $\beta(t) < -\mu_L$ for $t \in (t_1, t_2)$. From Fig. 6, $\dot{\beta}(t_1) = -\dot{\beta}(t_2) = -\sqrt{\lambda^2 - 1}$. Using the equation of the ellipse corresponding to $\beta(t) < -\mu_L$ from (17), and since $\dot{\beta}(t) = \lambda \sin(\alpha(t) - \phi)$, the coordinates $(\beta, \dot{\beta})$ of a point P_L on the ellipse can be parameterized in terms of the heading angle $\alpha(t)$ as

$$P_L = (-r_L - \mu_L - \lambda r_L \cos(\alpha(t) - \phi), \lambda \sin(\alpha(t) - \phi)). \tag{18}$$

Comparing the obtained expressions for β and $\dot{\beta}$ at t_1 and t_2 with (18), $\cos(\alpha(t_1) - \phi) = \cos(\alpha(t_2) - \phi) = \frac{-1}{\lambda}$, and $\sin(\alpha(t_1) - \phi) = -\sin(\alpha(t_2) - \phi) = -\frac{\sqrt{\lambda^2 - 1}}{\lambda}$. Since $\dot{\alpha}(t) = U_L > 0$ over an L segment, $\alpha(t) = \alpha(t_1) + U_L(t - t_1) > \alpha(t_1)$. Hence, the angles $\alpha(t_1) - \phi, \alpha(t_2) - \phi$, and the angle of the L segment (ϕ_L) can be represented as shown in Fig. 7. Therefore, $\phi_L = 2\pi - 2\theta = 2\pi - 2\cos^{-1}(\frac{1}{\lambda})$. Hence, $\phi_L \in (\pi, 2\pi)$.

The angle of the R segment of a non-trivial optimal SRS path can be derived similarly.

For a more detailed proof and the extension of the proof for the SRS path, the reader may refer to [18]. ■

Lemma 13: For $\lambda > e = 1$, the length of the line segment (l_S) of a non-trivial optimal LSR or RSL path is $\frac{\mu_L+\mu_R}{\sqrt{\lambda^2-1}}$.

Proof: For a non-trivial optimal LSR path with the first and second inflection points occurring at time instants t_1 and t_2, respectively,

- $\beta(t_1) = -\mu_L$ and $\beta(t_2) = \mu_R$ using Proposition 3,
- $\dot{\beta}(t) = \sqrt{\lambda^2-1}, t \in [t_1, t_2]$, using Proposition 10, and
- $l_S = t_2 - t_1 = \frac{\beta(t_2)-\beta(t_1)}{\sqrt{\lambda^2-1}} = \frac{\mu_L+\mu_R}{\sqrt{\lambda^2-1}}$, as the vehicle is considered to move at a unit speed.

A similar proof applies for the RSL path. For a more detailed proof, the reader may refer to [18]. ■

Lemma 14: For $\lambda > e = 1$, an optimal path contains at most five segments.

Proof: From Proposition 10, four candidate six-segment paths can be obtained, which are $LSRSLS$, $SRSLSR$, $RSLSRS$, and $SLSRSL$. Consider a non-trivial optimal $SLSRSL$ path. Using Lemmas 12 and 13, the $LSRS$ subpath is completely parameterized using λ. In particular, the angles of the L and R segments of this subpath are equal. Without loss of generality, let the initial and final configuration connected by this $LSRS$ subpath be such that

1) The center of the circle corresponding to the L segment is at the origin, and
2) The initial heading angle is $\frac{3\pi}{2}$.

As the L and R segments have an equal angle, the final heading angle is also $\frac{3\pi}{2}$. An alternate $SLSR$ path, constructed by removing the final S segment in the $LSRS$ subpath and inserting it before the LSR subpath, can connect the same initial and final configurations at the same cost. The considered initial position (P_i), the obtained final position (P_f), and the $LSRS$ and $SLSR$ paths are shown in Fig. 8.

Hence, from the initial non-trivial $SLSRSL$ path, an alternate non-trivial $SSLSRL$ path can be constructed connecting the same initial and final configurations at the same cost. However, using Corollary 11, the non-trivial $SSLSRL$ path is non-optimal, as it contains a non-trivial CC subpath. Hence, the non-trivial $SLSRSL$ path is not optimal. By string reversal, a non-trivial $LSRSLS$ path is not optimal. Using similar arguments, non-trivial $SRSLSR$ and $RSLSRS$ paths can be shown to be non-optimal. Hence, for $\lambda > e = 1$, an optimal path contains at most five segments. For a more detailed proof, the reader may refer to [18]. ■

Lemma 15: For $\lambda > e = 1$, there exists optimal four-segment paths of the same cost as non-trivial $SLSRS$ and $SRSLS$ paths.

Proof: Consider a non-trivial optimal $SLSRS$ path. Using Lemmas 12 and 13, the LSR subpath is parameterized using λ. Hence, the angles of the L and R segments are equal. The $LSRS$ subpath of the $SLSRS$ path can be replaced by an $SLSR$ path at the same cost using a similar construction used in the proof of Lemma 14. Hence, an alternate $SLSR$ path can be constructed with the same cost connecting the same initial and final configurations as the $SLSRS$ path. A similar argument follows for a non-trivial $SRSLS$ path. Hence, non-trivial $SLSRS$ and $SRSLS$ paths are redundant and need not be considered as candidate optimal paths. For a more detailed proof, the reader may refer to [18]. ■

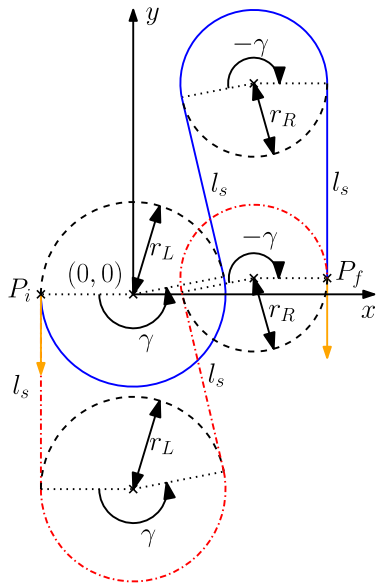

Fig. 8. Configurations connected by an $LSRS$ path and an alternate $SLSR$ path parameterized using a single parameter.

TABLE I
LIST OF CANDIDATE PATHS FOR THE WEIGHTED MARKOV-DUBINS PROBLEM

No. of segments	Candidate paths	No. of paths
1	S, C	3
2	SC, CS, CC	6
3	CSC, SCS	6
4	$LSRS$, $SRSL$, $RSLS$, $SLSR$	4
5	$LSRSL$, $RSLSR$	2

Theorem 16: There are at most 21 candidate paths for the minimum cost path for the weighted Markov-Dubins problem, which are given in Table I.

Remark 2: For $\mu_L = \mu_R = 0$, the list of candidate paths in Table I reduces to paths of type CSC, CCC, and degenerate paths of the same. This is because the length of an intermediate S segment in an optimal four or five-segment path tends to zero as $\mu_L, \mu_R \to 0$ from Lemma 13. Hence, the weighted Markov-Dubins problem generalizes the classical Markov-Dubins problem [1] and the asymmetric sinistral/dextral Markov-Dubins problem [13].

IV. RESULTS

A. Path Construction and Optimal Path for Teardrop Maneuver

Given the list of candidate paths in Table I, each candidate path should be generated (if it exists) for given initial and final configurations, vehicle parameters, and penalties. For this purpose, the approach used in [8] is adapted to derive closed-form expressions for the parameters of a given path, which are the

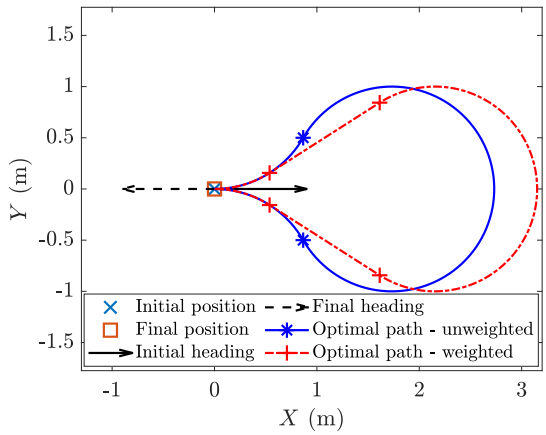

Fig. 9. Comparison of optimal paths for $r_L = r_R = 1$ m without weights and with $\mu_L = \mu_R = 1$.

angles for each L and R segment and the length of an S segment. The derivations use a corollary of Lemmas 12 and 13, wherein each candidate four and five-segment paths are parameterized by at most three parameters. For example, for an optimal $LSRSL$ path, consider angles ϕ_1, ϕ_2, and ϕ_3, for the first L segment, the R segment, and the final L segment, respectively. Using Lemma 12, λ can be expressed as a function of ϕ_2. As the length of the S segments is a function of λ, μ_L, and μ_R using Lemma 13, it can be expressed as a function of ϕ_2, μ_L, and μ_R. Hence, three parameters completely describe the $LSRSL$ path.

Consider the initial and final position of the vehicle to be at the origin and the initial and final headings to be 0° and 180°, respectively. Let $r_L = r_R = 1$ m. For the unweighted Markov-Dubins problem, the LRL path is optimal. However, it is not optimal with the introduction of weights. For $\mu_L = \mu_R = 1$, which corresponds to a 100% penalty imposed on turns, an $LSRSL$ path is optimal. The two cases are shown in Fig. 9. For the LRL path, the angles of the L and R segments are 60° and 300°, respectively. With the introduction of the penalties, the angles of the L and R segments are reduced to 32.53° and 245.07°, respectively, for the $LSRSL$ path due to the S segments, which are of length 1.28 m. Since an S segment is of lower cost than L and R segments, the resultant $LSRSL$ path is of a lower cost compared to an LRL path for the weighted case.

B. Effect of Parameters on Optimal Path Type

In this analysis, the previously considered (teardrop) maneuver was used to analyze the optimal path type for varying r_L, μ_L, r_R, and μ_R. Without loss of generality, r_L was set to one. Two values for μ_L were considered: 0, and 1, which correspond to no penalty and a 100% penalty for the left turn, respectively. The optimal path obtained for variations in r_R and μ_R in the range $[0.5, 3]$ m and $[0, 4]$, respectively, for the two values of μ_L are shown in Fig. 10. It can be observed that CCC paths are optimal only for $\mu_L = \mu_R = 0$, and are replaced with $CSCSC$ paths with a variation in a penalty. Moreover, for a large μ_R, an LSL path is optimal for $\mu_L = 0$ due to high right turn cost, and the $RSLSR$ path is observed to be optimal for $\mu_L = 1$.

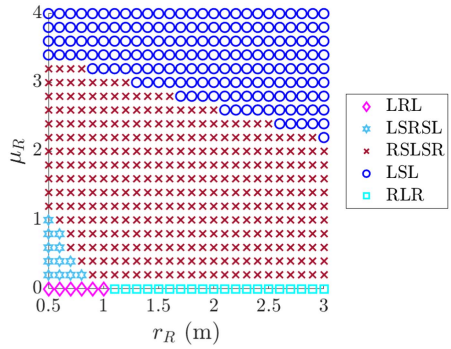

(a) $r_L = 1$ m, $\mu_L = 0$

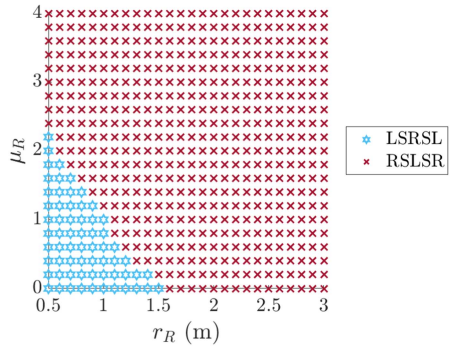

(b) $r_L = 1$ m, $\mu_L = 1$

Fig. 10. Parametric study of the optimal path for teardrop maneuver.

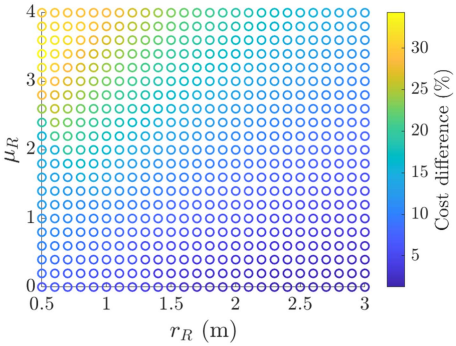

Fig. 11. Cost difference obtained considering only CSC and CCC paths for teardrop maneuver with $r_L = 1$ m, $\mu_L = 1$.

The novelty of the derived candidate paths can be further observed by considering the additional cost incurred by considering only the CSC and CCC paths (and degenerate paths) as candidate paths for the weighted problem. The cost difference, which represents the deviation from the optimum, is shown in Fig. 11 for the teardrop maneuver with $\mu_L = 1$. It can be observed that the deviation is, at most, about 34%.

C. Effect on Configurations on Optimal Path Type

In this analysis, the parameters of the vehicle were fixed, and the configurations were varied to study its effect on the optimal path type. The initial position was considered to coincide with the origin, and the initial heading angle was set to 0 radians. Similar to [13], the final heading angle of the vehicle was fixed

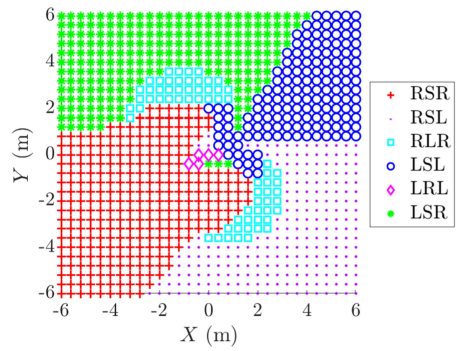

(a) $\mu_L = \mu_R = 0$

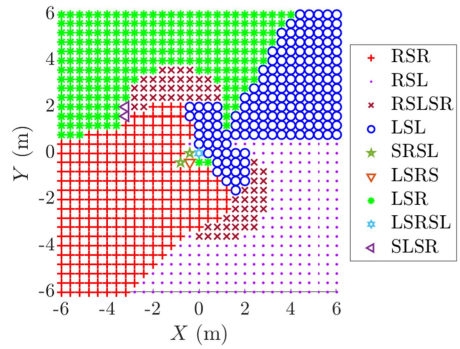

(b) $\mu_L = 0, \mu_R = 0.1$

Fig. 12. Effect of configuration on the optimal path type for $r_L = 1$ m, $r_R = 1.2$ m with final heading angle $= \frac{\pi}{3}$ radians.

to be $\frac{\pi}{3}$ radians, and the final position (x_f, y_f) was varied in $[-6, 6]$ m $\times [-6, 6]$ m. Considering $r_L = 1$ m, $r_R = 1.2$ m, with $\mu_L = \mu_R = 0$, the same result obtained in [13] is obtained, and is shown in Fig. 12(a). However, increasing μ_R from 0 to 0.1 results in the following changes:

- The RLR path being replaced by a path of type $RSLSR$, $SLSR$, or LSL.
- The LRL path being replaced by a path of type $SRSL$, $LSRSL$, $LSRS$, or LSL.
- Increased number of final positions close to origin that are optimally reached by the LSL path.

The optimal path for different final positions for $\mu_L = 0, \mu_R = 0.1$ is shown in Fig. 12(b).

V. Conclusion

In this letter, a variant of the classical Markov-Dubins problem, referred to as *weighted Markov-Dubins problem*, is addressed. The considered problem addresses curvature-constrained planar least-cost paths connecting given initial and final configurations with different bounds of the curvature for sinistral and dextral turns, and penalties μ_L and μ_R associated with those turns, respectively. The proposed problem is solved using Pontryagin's minimum principle. A total of 21 candidate optimal paths are obtained, each comprising at most five segments. Moreover, when $\mu_L = \mu_R = 0$, the candidate paths reduce to paths of type CSC and CCC and degenerate paths of the same. Hence, the addressed weighted Markov-Dubins problem generalizes the classical Markov-Dubins problem and the asymmetric sinistral/dextral Markov-Dubins problem. Finally, simulation results are presented to illustrate the novelty of the paths obtained over the paths for the classical Markov-Dubins problem and the asymmetric sinistral/dextral Markov-Dubins problem.

Acknowledgment

The authors gratefully acknowledge Christopher Montez, Texas A&M University, for useful discussions.

Distribution Statement A: Approved for public release, distribution unlimited. Case Number: AFRL-2022-3975.

References

[1] L. E. Dubins, "On curves of minimal length with a constraint on average curvature, and with prescribed initial and terminal positions and tangents," *Amer. J. Math.*, vol. 79, pp. 497–516, 1957.
[2] J. A. Reeds and L. A. Shepp, "Optimal paths for a car that goes both forwards and backwards," *Pacific J. Math.*, vol. 145, pp. 367–393, 1990.
[3] L. S. Pontryagin, V. G. Boltyanskii, R. V. Gamkrelidze, and E. F. Mishchenko, *The Mathematical Theory of Optimal Processes*. New York, NY, USA: Interscience Publishers, 1962.
[4] H. J. Sussmann and G. Tang, "Shortest paths for the Reeds-Shepp car: A worked out example of the use of geometric techniques in nonlinear optimal control," Rutgers University, New Brunswick, NJ, USA, Tech. Rep. SYCON91-10, 1991.
[5] J.-D. Boissonnat, A. Cerezo, and J. Leblond, "Shortest paths of bounded curvature in the plane," in *Proc. IEEE Int. Conf. Robot. Automat.*, 1992, pp. 2315–2320.
[6] C. Y. Kaya, "Markov–Dubins path via optimal control theory," *Comput. Optim. Appl.*, vol. 68, pp. 714–747, 2017.
[7] X.-N. Bui, J.-D. Boissonnat, P. Soueres, and J.-P. Laumond, "Shortest path synthesis for Dubins non-holonomic robot," in *Proc. IEEE Int. Conf. Robot. Automat.*, 1994, pp. 2–7.
[8] A. M. Shkel and V. Lumelsky, "Classification of the Dubins set," *Robot. Auton. Syst.*, vol. 34, pp. 179–202, 2001.
[9] P. Soueres and J.-P. Laumond, "Shortest paths synthesis for a car-like robot," *IEEE Trans. Autom. Control*, vol. 41, no. 5, pp. 672–688, May 1996.
[10] F. Monroy-Pérez, "Non-euclidean Dubins' problem," *J. Dyn. Control Syst.*, vol. 4, pp. 249–272, 1998.
[11] H. Sussmann, "Shortest 3-dimensional paths with a prescribed curvature bound," in *Proc. IEEE 34th Conf. Decis. Control*, 1995, pp. 3306–3312.
[12] S. G. Manyam, D. W. Casbeer, A. V. Moll, and Z. Fuchs, "Shortest Dubins paths to intercept a target moving on a circle," *J. Guid., Control, Dyn.*, vol. 45, pp. 2107–2120, 2022.
[13] E. Bakolas and P. Tsiotras, "The asymmetric sinistral/dextral Markov-Dubins problem," in *Proc. IEEE 48th Conf. Decis. Control*, 2009, pp. 5649–5654.
[14] M. H. Sadraey, *Aircraft Design: A Systems Engineering Approach*. Hoboken, NJ, USA: Wiley, 2012, ch. 12.
[15] Pilot's Handbook of Aeronautical Knowledge, U. S. *Department of Transportation - Federal Aviation Administration*, ch. 5, pp. 1–15, 2016.
[16] M. Athans and P. L. Falb, *Optimal Control: An Introduction to the Theory and Its Applications*. New York, NY, USA: Dover Publications, 2006.
[17] P. D. Loewen, "The pontryagin maximum principle," 2012. [Online]. Available: https://personal.math.ubc.ca/~loew/m403/pmp.pdf
[18] D. P. Kumar, S. Darbha, S. G. Manyam, and D. Casbeer, "*The Weighted Markov-Dubins Problem*," 2022, *arXiv:2211.06908*.